63rd International Astronautical Congress, Naples, Italy. Copyright ©2012 by Steven Owens. Published by the IAF, with permission and released to the IAF to publish in all forms".

IAC-12-C1.5.5

AN EXTENSION AND NUMERICAL ANALYSIS OF THE HOHMANN SPIRAL TRANSFER

Steven Owens
Advanced Space Concepts Laboratory/University of Strathclyde, Glasgow, Scotland,
steven.owens@strath.ac.uk

Malcolm Macdonald
Advanced Space Concepts Laboratory/University of Strathclyde, Glasgow, Scotland,
malcolm.macdonald.102@strath.ac.uk

This paper extends previous work on the Hohmann Transfer Spiral (HST) by introducing a plane change into the analysis. An analytical expression determining the critical specific impulse incorporating a plane change is derived for both a circular and elliptical initial orbit. This expression determines the point at which the HST is equivalent in terms of fuel mass fraction to the compared Hohmann transfer. The expression assumes that the inclination change is performed by the high-thrust system. The numerical approach uses a blending method coupled with optimised weighting constants to deliver a locally optimal low-thrust trajectory. By comparing the analytical and numerical approaches, it is shown that the analytical can deliver a good estimation of the HST characteristics so long as little orbit eccentricity control is required. In the cases where orbit eccentricity control is required, the numerical approach should be used. A case study from an inclined Geostationary Transfer Orbit, equivalent to a high-latitude launch site, to Geostationary Earth Orbit has shown that the HST can offer a fuel mass saving approximately 5% of the launch mass. This equates to the mass penalty associated with this high-latitude launch site and therefore mimics the advantages of a low-latitude launch site at the expense of a longer transfer duration.

I.NOMENCLATURE

g – standard gravitational acceleration, m/s^2

g_r – gravitational acceleration at specified radius

μ - gravitational constant, km^3/s^2

m_{dry} – spacecraft mass without fuel, kg

m_{wet} – spacecraft mass with total fuel, kg

m_{dry}– spacecraft mass delivered on orbit, kg

m_{highF} – high-thrust system fuel mass, kg

m_{HSTLF} – HST low-thrust section fuel mass, kg

m_{HSTF} – HST fuel mass, kg

m – instantaneous spacecraft mass, kg

m_{02} – spacecraft mass after phase 1 of the HST transfer, kg

ΔV_{TIhigh} – high-thrust only system with inclination change ΔV(circular initial orbit), m/s

ΔV_{TIH} – high-thrust portion of HST with inclination change ΔV(circular initial orbit), m/s

ΔV_L – low-thrust portion of HST ΔV, m/s

$\Delta V_{TIEhigh}$ – high-thrust only system with inclination change ΔV (elliptical initial orbit), m/s

ΔV_{TIEH} – high-thrust section of HST with inclination change ΔV (elliptical initial orbit), m/s

I_{spH} – high-thrust system specific impulse, s

I_{spL} – low-thrust system specific impulse, s

I_{sp}^{HHH-} – Hohmann and HST critical specific impulse ratio (circular initial orbit)

I_{sp}^{HHHE} – Hohmann and HST critical specific impulse ratio (elliptical initial orbit)

$\Delta V_{a/a'/b/b'}$ – specified node ΔV between transfer and initial, m/s

$v_{initial}$ – initial orbit velocity at beginning of specified transfer, m/s

v_{final} – target/intermediate orbit velocity at end of specified transfer, m/s

$v_{transa/b(a'/b')}$ – transfer orbit velocity at specified node, m/s

ΔI – total inclination change, radians

s – percentage of inclination change at node a/a'

r – Instantaneous radius of spacecraft

r_i – initial orbit radius, km

r_t – target orbit radius, km

r_c – circular transfer orbit, km

a_1 – semi-major axis between r_i and r_c

acc – spacecraft acceleration, m/s^2

T – spacecraft thrust, mN

$R2^*$ – critical R2

t – time, days

t_T – total HST transfer duration, days

t_1 – HST transfer phase 1 duration (high-thrust), days

t_2 – HST transfer phase 2 duration (low-thrust), days

λ_σ– locally optimal orientation vector for element σ

λ_b– locally optimal orientation blended vector

W_σ– optimised weighting constant for each element σ

p – semi-latus rectum, km

a – semi-major axis, km

e – eccentricity

υ – true anomaly, radians

E – eccentric anomaly

f – modified equinoctial element

g – modified equinoctial element

L – modified equinoctial element

II.INTRODUCTION

This paper extends previous work[1], which introduced the Hohmann Spiral Transfer (HST) as a hybrid propulsion transfer utilising both high and low-thrust systems, by introducing a plane change into the analysis. Previously, research in the area of hybrid propulsion transfers has focused on a transfer in which the low thrust system is activated at a point between the initial and final orbit[2–4]. The HST is similar to the bi-elliptic transfer as the high-thrust system is first used to propel the spacecraft way beyond the target orbit while also changing part of the inclination. At an intermediate orbit the high-thrust system is used to enter a circular orbit with radius, r_c, as shown in Figure 1 while also completing the inclination change to give the desired orbital plane. The low-thrust system is then activated and the spacecraft is propelled on an inward spiral trajectory towards its target orbit. This paper first introduces an analytical expression that describes, by way of a critical specific impulse ratio, the point at which the HST transfer consumes the same amount of fuel as the high-thrust only transfer for both a circular and elliptical initial orbit. It then goes on to determine the characteristics of these equations for a range of intermediate orbits and inclination changes before validating them with a numerical analysis. A method for restraining the time is introduced and then applied to a case study in which the HST is used for transfer between a Geostationary Transfer Orbit (GTO) and Geostationary Earth Orbit (GEO). The following assumptions are applied throughout the analytical analysis; finite burn losses are ignored and only the gravitational force of the Earth is considered.

III.CRITICAL SPECIFIC IMPULSE DERIVATION

The following equations derive the critical specific impulse ratio, which can then be applied to each case independently. The high thrust and HST fuel mass fractions can be written as

$$\frac{m_{highF}}{m_{wet}} = 1 - exp^{\left(\frac{-\Delta V_{TIhigh}}{gI_{spH}}\right)} \quad (1)$$

$$\frac{m_{HSTF}}{m_{wet}} = 1 - exp^{\left(\frac{-\Delta V_{TIH}}{gI_{spH}}\right)} exp^{\left(\frac{-\Delta V_{L}}{gI_{spL}}\right)} \quad (2)$$

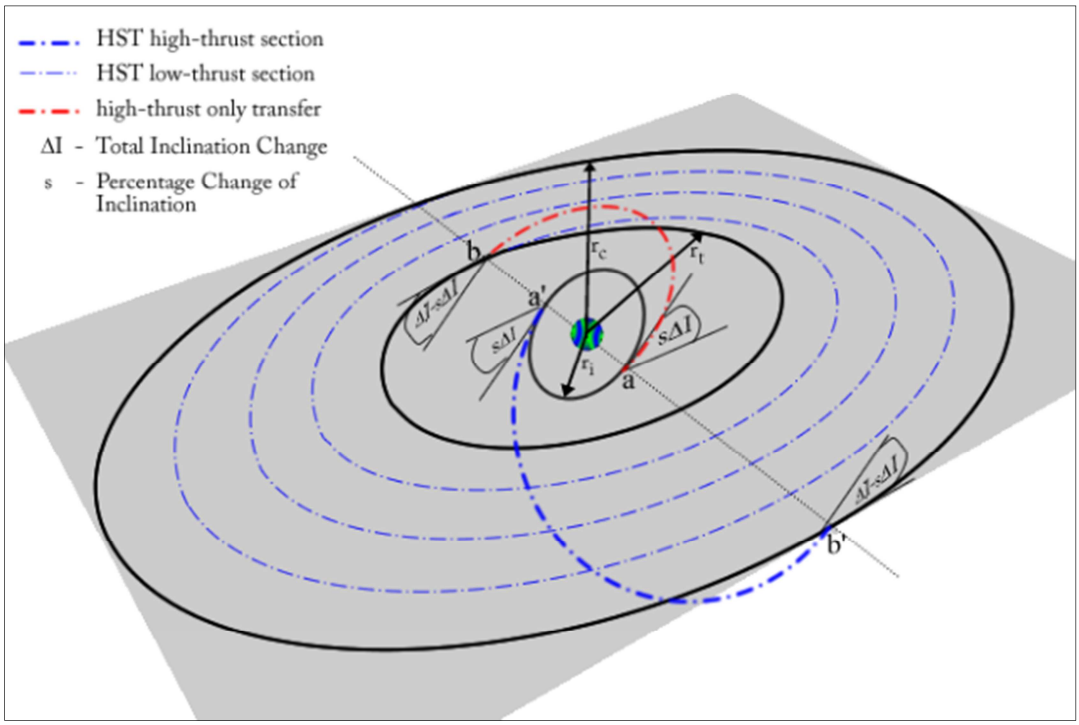

Figure 1 Three-Dimensional Hohmann Spiral Transfer (HST) representation

By equating Eqs. (1) and (2), it can be shown that the HST is equivalent or better in terms of fuel mass fraction when

$$exp\left(\frac{-\Delta V_{TIhigh}}{gI_{spH}}\right) \leq exp\left(\frac{-\Delta V_{TIH}}{gI_{spH}}\right) exp\left(\frac{-\Delta V_{L}}{gI_{spL}}\right) \quad (3)$$

which can be simplified to give

$$\frac{I_{spL}}{I_{spH}} \geq \frac{\Delta V_L}{\Delta V_{TIhigh} - \Delta V_{TIH}} \quad (4)$$

confirming that a critical specific impulse ratio can be determined for the condition when the high-thrust fuel consumption is equal to the HST fuel consumption. Thus, for a given set of initial conditions, any specific impulse ratio above this critical value will mean the HST is more fuel-efficient than the high-thrust only transfer.

From Eq. (4) it can be seen that, for the condition when the HST high-thrust required change in velocity, ΔV, equals that of the high-thrust only ΔV, a singularity exists. Beyond this signifies the region where the HST requires more fuel than the High-thrust only transfer and would be required to add mass to the system rather than remove it. Due to this singularity, all figures within this paper are bound to regions deemed feasible for both current and near-future propulsion capabilities[5–7].

IV. THREE-DIMENSIONAL VELOCITY CHANGE ANALYTICAL METHODOLOGY

As is commonly known, it is more efficient to impart a plane change and orbit raise as part of the same manoeuvre, compared to carrying out each sequentially, when using a high-thrust system[8]. The ΔV required to perform the transfer is therefore calculated by comparing the initial and final orbit velocity vectors as well as the inclination plane change required. This is done using the cosine law as part of vector analysis. Figure 1 highlights the transfer specification while Eq. (5) details the ΔV equation.

$$\Delta V_{a/b(a'/b')} = \sqrt{v_{initial/final}{}^2 + v_{trans_{a/b}}{}^2 - 2v_{initial/final}v_{trans_{a/b}}\cos(\Delta I)} \quad (5)$$

As the transfer is conducted using two impulses, one to enter the transfer orbit and one to capture the target orbit, the question then arises as to how much inclination change to impart at each impulse of the manoeuvre. An analytical approximation of this has already been established to an accuracy of 0.5° which introduces a scaling term, *s*, to represent the inclination imparted at each impulse as shown in Eq. (6)[9].

$$\Delta V = \Delta V_{a/a'} + \Delta V_{b/b'} = \sqrt{v_{initial}{}^2 + v_{trans_{a/a'}}{}^2 - 2v_{initial}v_{trans_{a/a'}}\cos(s\Delta I)} + \quad (6)$$

$$\sqrt{{v_{final}}^2 + {v_{trans_{b/b'}}}^2 - 2v_{final}v_{trans_{b/b'}}\cos((1-s)\Delta I)}$$

Firstly, squaring the two velocities to remove the square roots and ignoring the cross product terms ($2\Delta V_a \Delta V_b$) gives

$${\Delta V_{a/a'}}^2 + {\Delta V_{b/b'}}^2 \approx {v_{initial}}^2 + {v_{trans_{a/a'}}}^2 -$$
$$2v_{initial}v_{trans_{a/a'}}\cos(s\Delta I) + {v_{fin\,al}}^2 +$$
$${v_{trans_{b/b'}}}^2 - 2v_{final}v_{trans_{b/b'}}\cos\big((1-s)\Delta I\big)$$

This can then be differentiated with respect to s and set equal to zero:

$$\frac{\partial\big({\Delta V_{a/a'}}^2 + {\Delta V_{b/b'}}^2\big)}{\partial s}$$
$$\approx \Delta I 2v_{initial}v_{trans_{a/a'}}\sin(s\Delta I)$$
$$-\Delta I 2v_{final}v_{trans_b}\sin\big((1-s)\Delta I\big) = 0$$

By collecting terms and rearranging:

$$\frac{\sin(s\Delta I)}{\cos(s\Delta I)} \approx \frac{v_{final}v_{trans_{b/b'}}\sin(\Delta I)}{v_{initial}v_{trans_{a/a'}} + v_{final}v_{trans_{b/b'}}\cos(\Delta I)}$$

Which then, with further simplication gives

$$s \approx \frac{1}{\Delta I}\tan^{-1}\left[\frac{\sin(\Delta I)}{X+\cos(\Delta I)}\right] \quad (7)$$

Where $X = \frac{v_{initial}v_{trans_{a/a'}}}{v_{final}v_{trans_{b/b'}}}$

Note that X can be modified, depending on the transfer scenario under consideration, by introducing the velocity formulas and simplifying with respect to the orbit ratios. For each transfer considered in this section this is accounted for and X is adjusted accordingly.

V.CIRCULAR INITIAL ORBIT

Considering Figure 1 and Eq. (4), Eqs.(8),(9) and (10) give the required ΔV for the low-thrust transfer section of the HST, the high-thrust section of the HST responsible for both the transfer and inclination change and the high-thrust only Hohmann transfer, also responsible for the transfer and inclination change, respectively. It should be noted Eq. (8) is an approximate expression for the low-thrust ΔV.

$$\Delta V_L = \sqrt{\frac{\mu}{r_t}} - \sqrt{\frac{\mu}{r_c}} \quad (8)$$

$$\Delta V_{TIH} = \sqrt{\frac{\mu}{r_i} + \frac{2\mu r_c}{r_i(r_i+r_c)} - 2\sqrt{\frac{\mu}{r_i}}\sqrt{\frac{2\mu r_c}{r_i(r_i+r_c)}}cos(\Delta I_{a'})} + \sqrt{\frac{\mu}{r_c} + \frac{2\mu r_i}{r_c(r_i+r_c)} - 2\sqrt{\frac{\mu}{r_c}}\sqrt{\frac{2\mu r_i}{r_c(r_i+r_c)}}cos(\Delta I_{b'})} \quad (9)$$

$$\Delta V_{TIhigh} = \sqrt{\frac{\mu}{r_i} + \frac{2\mu r_t}{r_i(r_i+r_t)} - 2\sqrt{\frac{\mu}{r_i}}\sqrt{\frac{2\mu r_t}{r_i(r_i+r_t)}}cos(\Delta Ia)} + \sqrt{\frac{\mu}{r_t} + \frac{2\mu r_i}{r_t(r_i+r_t)} - 2\sqrt{\frac{\mu}{r_t}}\sqrt{\frac{2\mu r_i}{r_t(r_i+r_t)}}cos(\Delta Ib)} \quad (10)$$

Where

$$\Delta I_{a'/a} = s\Delta I = tan^{-1}\left[\frac{sin(\Delta I)}{\frac{\sqrt{\frac{\mu}{r_i}}\sqrt{\frac{2\mu r_{c/t}}{r_i(r_i+r_{c/t})}}}{\sqrt{\frac{\mu}{r_{c/t}}}\sqrt{\frac{2\mu r_i}{r_{c/t}(r_i+r_{c/t})}}} + cos(\Delta I)}\right] \quad (11)$$

and

$$\Delta I_{b'/b} = (1-s)\Delta I = \Delta I - tan^{-1}\left[\frac{sin(\Delta I)}{\frac{\sqrt{\frac{\mu}{r_i}}\sqrt{\frac{2\mu r_{c/t}}{r_i(r_i+r_{c/t})}}}{\sqrt{\frac{\mu}{r_{c/t}}}\sqrt{\frac{2\mu r_i}{r_{c/t}(r_i+r_{c/t})}}} + cos(\Delta I)}\right] \quad (12)$$

By then introducing the orbit ratios $R1\left(=\frac{r_t}{r_i}\right)$ and $R2\left(=\frac{r_c}{r_i}\right)$, Eq. (4) reduces to give

$$\frac{I_{spL}}{I_{spH}} = {I_{sp}}^{HHH-} = \frac{1-\sqrt{\frac{R1}{R2}}}{\sqrt{R1}\left[\mathcal{A}_1-\mathcal{A}_2-\sqrt{\frac{1}{R2}}\mathcal{A}_3\right]+\mathcal{A}_4} \qquad (13)$$

Where

$$\mathcal{A}_1 = \sqrt{1+\frac{2R1}{1+R1}-\sqrt{\frac{8R1}{1+R1}}cos\left(tan^{-1}\left[\frac{sin(\Delta I)}{\sqrt{(R1)^3}+cos(\Delta I)}\right]\right)}$$

$$\mathcal{A}_2 = \sqrt{1+\frac{2R2}{1+R2}-\sqrt{\frac{8R2}{1+R2}}cos\left(tan^{-1}\left[\frac{sin(\Delta I)}{\sqrt{(R2)^3}+cos(\Delta I)}\right]\right)}$$

$$\mathcal{A}_3 = \sqrt{1+\frac{2}{1+R2}-\sqrt{\frac{8}{1+R2}}cos\left(tan^{-1}\left[\Delta I-\frac{\sin(\Delta I)}{\sqrt{(R2)^3}+cos(\Delta I)}\right]\right)}$$

$$\mathcal{A}_4 = \sqrt{1+\frac{2}{1+R1}-\sqrt{\frac{8}{1+R1}}cos\left(tan^{-1}\left[\Delta I-\frac{sin(\Delta I)}{\sqrt{(R1)^3}+cos(\Delta I)}\right]\right)}$$

Eq. (13) depends on *R1*, *R2* and ΔI and in the case where the target orbit radius and inclination are known, the equation depends on only *R2* or more specifically, the intermediate circular orbit radius value, r_c. Varying this will give a range of transfer orbits with a given critical ratio defining the point where the HST, using the high-thrust system to impart the inclination change, is equivalent in terms of fuel mass fraction to that of the Hohmann transfer. Figure 2 and 3 highlight the characteristics of this critical ratio with Figure 2 showing varying *R2* as well as Inclination. It can be seen that with increasing inclination for all *R2* values ${I_{sp}}^{HHH-}$ drops off with an increasing inclination change suggesting that the greater the inclination change the more beneficial the HST transfer is. Figure 3 shows ${I_{sp}}^{HHH-}$ for a fixed *R1* and *R2* with changing inclination and highlights again the drop in critical ratio with increasing inclination change but also shows that the critical ratio tends to a constant value with an inclination change above approximately 1.6radians (90°). For Figure 2 and 3 *R1*=6.36 as this represents a GTO to GEO transfer and *R2*=100 in Figure 3 as this highlights the common characteristics of the critical equation at large *R2* values.

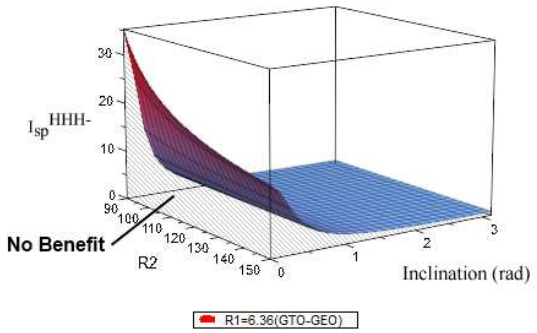

Figure 2 ${I_{sp}}^{HHH-}$ Characteristics (R1=6.36)

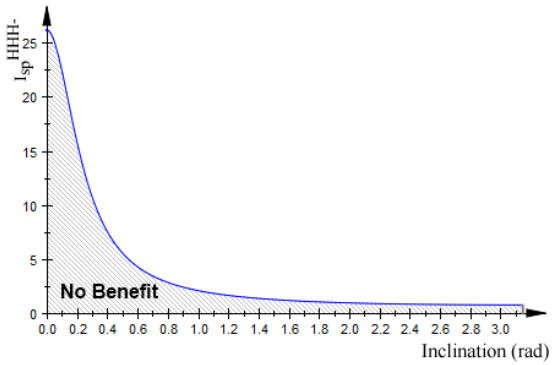

Figure 3 ${I_{sp}}^{HHH-}$ Characteristics (R1=6.36, R2=100)

VI.ELLIPTICAL INITIAL ORBIT

Considering Figure 4, detailing the elliptical starting orbit it is clear for the high-thrust Hohmann case, as the starting orbit apogee coincides with the target orbit, only one impulse is required to capture the target orbit. The direction and magnitude of this impulse is therefore dependent on the final orbit radius and inclination change required. This scenario is used as it representative of a transfer from a Geostationary Transfer Orbit (GTO) to a Geostationary Earth Orbit (GEO)[10]. In order to determine the impulse it can be broken up into two components, the orbit raising component and the plane change component, as shown in Figure 4.

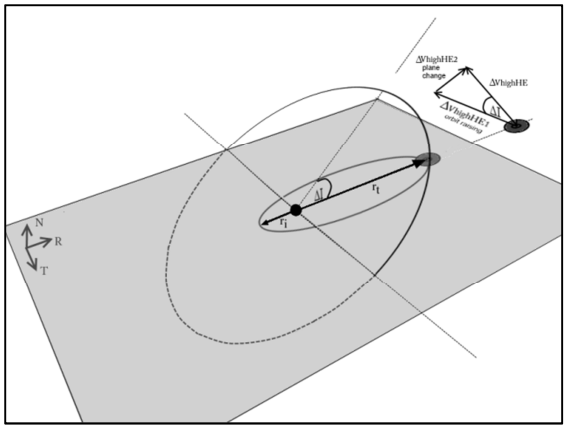

Figure 4 Single Impulse High-thrust transfer to Capture Target Orbit

Applying the law of cosines theorem[11] gives the high-thrust only single impulse as shown in Eq. (14).

$$\Delta V_{TIEhigh} = \sqrt{\frac{2\mu r_i}{r_t(r_i+r_t)} + \frac{\mu}{r_t} - 2\sqrt{\frac{2\mu r_i}{r_t(r_i+r_t)}}\sqrt{\frac{\mu}{r_t}}\cos(\Delta I)} \quad (14)$$

The HST high-thrust section incorporating the plane change and now accounting for the elliptical initial orbit is given in Eq. (15). The orbit ratios, as previously defined, are used for simplification.

$$\Delta V_{TIEH} = \sqrt{\frac{\mu}{r_t}}\sqrt{\frac{R1}{R2}}\left(\sqrt{R2}\mathcal{B}_1 + \mathcal{B}_2\right) \quad (15)$$

Where

$$\mathcal{B}_1 = \sqrt{\frac{2R1}{1+R1} + \frac{2R2}{1+R2} - \sqrt{\frac{8R1}{1+R1}}\sqrt{\frac{2R2}{1+R2}}cos(\sigma_2)}$$

$$\mathcal{B}_2 = \sqrt{1 + \frac{2}{1+R2} - \sqrt{\frac{8}{1+R2}}cos(\Delta I - \sigma_2)}$$

$$\sigma_2 = tan^{-1}\left[\frac{sin(\Delta I)}{\sqrt{\frac{2R1R2^3}{1+R1}}+cos(\Delta I)}\right]$$

The low-thrust section of the HST transfer is the same as Eq. (8). Using these definitions, along with the orbit ratios as previously defined, and substituting into Eq. (4), the critical ratio for the scenario of a high-thrust only and HST comparison, where the initial orbit is elliptical and the inclination change is performed by the high-thrust section of the HST, is given in Eq. (16).

$$\frac{I_{spL}}{I_{spH}} = I_{sp}{}^{HHHE} = \frac{1-\sqrt{\frac{R1}{R2}}}{\mathcal{C}_1 - \sqrt{\frac{R1}{R2}}(\sqrt{R2}\mathcal{C}_2 + \mathcal{C}_3)} \quad (16)$$

Where

$$\mathcal{C}_1 = \sqrt{\frac{2}{1+R1} + 1 - 2\sqrt{\frac{2}{1+R1}}cos(\Delta I)}$$

$$\mathcal{C}_2 = \sqrt{\frac{2R1}{1+R1} + \frac{2R2}{1+R2} - \sqrt{\frac{8R1}{1+R1}}\sqrt{\frac{2R2}{1+R2}}cos\left(tan^{-1}\left[\frac{sin(\Delta I)}{\sqrt{\frac{2R1R2^3}{1+R1}}+cos(\Delta I)}\right]\right)}$$

$$\mathcal{C}_3 = \sqrt{1 + \frac{2}{1+R2} - \sqrt{\frac{8}{1+R2}}cos\left(\Delta I - tan^{-1}\left[\frac{sin(\Delta I)}{\sqrt{\frac{2R1R2^3}{1+R1}}+cos(\Delta I)}\right]\right)}$$

Similar to before, the critical ratio depends on only three variables, *R1*, *R2* and *ΔI*. If the target orbit and inclination are known then this equation depends on only *R2* or more specifically, the intermediate circular orbit radius value, r_c. Varying this will give a range of critical specific impulse ratios that determine when the HST is equivalent, in terms of fuel mass fraction, to the high-thrust only transfer. Figure 5 and 6 show the characteristics of $I_{sp}{}^{HHHE}$ and highlight the similarity with the circular initial orbit; that with increasing *ΔI* the critical ratio reduces suggesting that the HST's efficiency increases.

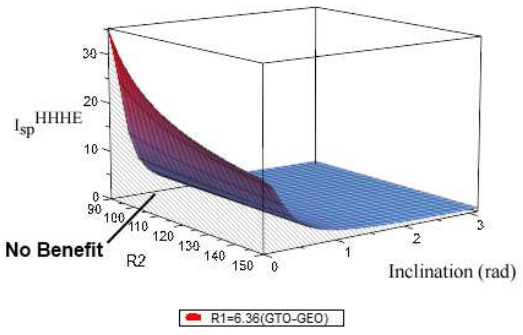

Figure 5 $I_{sp}{}^{HHHE}$ characteristics (R1=6.36)

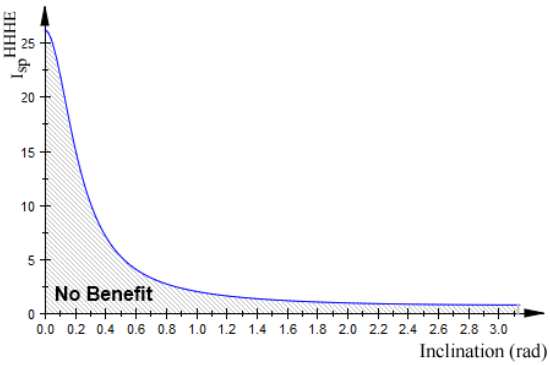

Figure 6 I_{sp}^{HHHE} characteristics (R1=6.36, R2=100)

VII. NUMERICAL METHOD AND LOCALLY OPTIMAL CONTROL LAWS USED

The optimisation method adopted in this paper is formulated using locally optimal control laws in the form of modified equinoctial elements [12]. These elements are non-singular except for rectilinear orbits and when $i=\pi$. In this paper, it is applicable to the low-thrust section of the HST.

Locally Optimal Control Laws

There are seven locally optimal control laws however only the semi-major axis and eccentricity are needed for this analysis so are derived in this section. As the rate of change of an element can be easily calculated, a locally optimal control law can be generated. These control laws aim to maximise the instantaneous rate of the element and provide the required thrust vector in a closed analytical form. The advantage of these control laws is the speed at which they can be implemented in trajectory models. The disadvantage is the sub-optimal nature of them and how this affects the resulting solution[13]. The variational equation of the element concerned can be described as shown in Eq. (17).

$$\frac{d\sigma}{dt} = \boldsymbol{f}.\hat{\boldsymbol{\lambda}}_{\boldsymbol{\sigma}} \tag{17}$$

where σ represents the respective element. The required force, $\boldsymbol{f}$, in the Radial, Transverse and Normal Axes (RTN) to maximise the rate of change of σ is a unit vector described by $\boldsymbol{\lambda}_{\sigma}$. By maximising the force along $\boldsymbol{\lambda}_{\sigma}$, the instantaneous rate of σ is also maximised.

Semi-Major Axis Control Law

The semi-major axis variational equation is given in Eq. (18) in classical elements

$$\frac{da}{dt} = \frac{2a^2}{\sqrt{\mu p}}\begin{bmatrix} R & T & N \end{bmatrix}\begin{bmatrix} esin(v) \\ 1 + esin(v) \\ 0 \end{bmatrix} \tag{18}$$

By then identifying $\boldsymbol{\lambda}_{\boldsymbol{a}}$ and converting to modified equinoctial elements, the maximised unit thrust direction vector is given in Eq. (19).

$$\lambda_a = \begin{bmatrix} esin(v) \\ 1 + esin(v) \\ 0 \end{bmatrix} = \begin{bmatrix} fsin(L) - gcos(L) \\ 1 + (fcos(L) + gsin(L)) \\ 0 \end{bmatrix} \tag{19}$$

This can now be used to generate a locally optimal control law which focuses on maximising the semi-major axis. This is also known as the energy gain control law as it gives a locally optimal variation in orbit energy.

Eccentricity Control Law

The eccentricity variational equation is given in Eq. (20) and is defined in classical elements.

$$\frac{de}{dt} = \frac{p}{\mu}\begin{bmatrix} R & T & N \end{bmatrix}\begin{bmatrix} \sin(v) \\ \cos(v) + \cos(E) \\ 0 \end{bmatrix} \tag{20}$$

By identifying $\boldsymbol{\lambda}_{\boldsymbol{e}}$ and converting to modified equinoctial elements, the maximised thrust direction vector is given in Eq. (21).

$$\lambda_e = \begin{bmatrix} \sin(v) \\ \cos(v) + \cos(E) \\ 0 \end{bmatrix} = \begin{bmatrix} \frac{fsin(L) - gcos(L)}{\sqrt{f^2+g^2}} \\ \frac{[fsin(L)+gcos(L)]\left[1+\frac{r}{p}\right]}{\sqrt{f^2+g^2}} + \frac{r\sqrt{f^2+g^2}}{p} \\ 0 \end{bmatrix} \tag{21}$$

Control Law Blending

The blending method used in this analysis is based on a form of averaging that has previously been applied to solar sail trajectory design and is known as A^nD blending[13]. The method is adopted here to suit low-thrust technologies without the limitations of a sail i.e. the thrust can be used in any direction as and when it is needed. The method calculates the deficit (time to target) of each control

law based on the maximised thrust vector if it were solely used and assuming a constant rate of change. These are then normalised with respect to the largest resulting with each control law receiving a score between zero and one, zero meaning the control law has achieved its target and one meaning it is furthest, in terms of time, from its target value. The control laws are then multiplied by an optimised weighting constant, based on mission specification, before finally being blended using the averaging technique as is shown in Eq. (22). This now forms the maximised thrust direction unit vector, all symbols have the same meanings as previously discussed.

$$\boldsymbol{\lambda_b} = \frac{\sum_\sigma W_\sigma \hat{\boldsymbol{\lambda}}_\sigma}{\sum_\sigma W_\sigma} \tag{22}$$

As opposed to several other blending methods in which the optimisation process calculates the weighting parameters as a function of time from the initial epoch[5,6], this method ensures that the optimised weighting constants are independent of time. It should be noted that as the low-thrust system is assumed to be always thrusting, the optimised constants deliver both a minimum time and fuel mass transfer.

Optimisation Method

The optimisation analysis in this paper uses the fmincon function, which is part of the Matlab® programming suite. Fmincon is a constrained nonlinear optimisation method adapting a sequential quadratic programming (SQP) method. SQP was selected as it has a strict feasibility with respect to the bounds meaning every iterative step is taken within the specified bounds[16]. This is necessary for this study as the constants cannot be negative otherwise the trajectory generation will fail. As a result the lower boundary remains always at zero.

Analytical and Numerical Validation

As the trajectory design optimisation is only concerned with the low-thrust section, the comparison only considers this section of the transfer. Table 1 gives the parameters used in the validation study.

HST Validation	
Initial Orbit (LEO), r_i (km)	6628
Target Orbit (GEO), r_t (km)	42154.08
Intermediate Orbit, r_c (km)	66380
R1	6.36
R2	10
Initial Mass, m_{wet} (kg)	554
High-thrust system specific impulse, I_{spH} (s)	325
Low-thrust system specific impulse, I_{spL} (s)	4500
Thrust, T (mN)	150
Inclination Change, ΔI (°)	7

Table 1 Validation Model Parameters

Table 2 gives the results of the comparison with the relative error under 3%. It should be noted that the numerical code is considered to have achieved the target orbit when it is within 1% of the target GEO. Both analyses are based on constant acceleration.

Orbit Parameter	Low-thrust fuel mass, m_{HSTF} (kg)	Low-thrust transfer time, t_2 (days)
Analytical	4.6	15.77
Numerical	4.52	15.39
Absolute Relative Error *w.r.t Numerical* (%)	1.77	2.47

Table 2 Co-Planar Comparison

As the relative error is under 3% the analytical method is deemed valid for use in gaining a basic understanding of the transfer characteristics.

VIII. TIME RESTRICTED TRANSFERS

The analysis so far has been independent of time in order to gain a basic insight into the operation of the system. In order to then analyse real life mission scenarios it is necessary to include the transfer time so that a reasonable comparison can be made to current transfer methods. This section introduces a method to restrict the HST with an overall transfer duration by extending Newton's second law, as given in Eq. (23), and substituting it into Eq. (2).

$$\Delta V_L = \frac{T}{m_{02}}(t_2) \tag{23}$$

Equation (24) and (25) introduce the time dependency for both the high and low-thrust sections of the HST while Eq. (26) allows the use of the orbit ratios previously defined. Thereafter substituting into Eq. (2) yields Eq. (27). As the inclination change ΔV is incorporated in the two high-thrust impulses of the HST there is no additional time requirement compared to the co-planar case.

$$t_T = t_1 + t_2 \tag{24}$$

$$t_1 = \pi\sqrt{\frac{{a_1}^3}{\mu}} \tag{25}$$

$$a_1 = \frac{r_t}{2R1}(1 + R2) \tag{26}$$

$$\frac{m_{HSTF}}{m_{wet}} = 1 - exp\left[\left(\frac{-\Delta V_{TIhigh}}{gIsp_H}\right) + \left(\frac{-\left(\frac{T}{m_{02}}\left(t_T - \frac{\pi}{\sqrt{\mu}}\sqrt{\left(\frac{rt(1+R2)}{2R1}\right)^3}\right)\right)}{gIsp_L}\right)\right] \tag{27}$$

Introducing a time constraint element introduces a dependency on the thrust of the low-thrust system to ensure the transfer is completed in the restricted time. This allows a mission design space to be created.

IX.CASE STUDY

Virtual Launch Site For High-Latitude Launch Port (Elliptical)

Analytical

When considering the HST with an inclination change it becomes clear that the transfer is more beneficial, compared against the conventional high-thrust Hohmann transfer, with a larger inclination change. This means that there may be significant benefit using the HST if the launch site is restricted to a high latitude and the target is GEO. This case study considers a satellite with a technological configuration given in Table 3 which is of similar specification to the new Alphabus[1] platform being developed to allow platforms with greater payload power and mass to accommodate the telecommunications market. It was selected as the platform already incorporates high and low-thrust propulsion systems and is therefore suitable for this analysis. Firstly it considers a launch from the Guiana Space Centre near Kourou in French Guiana and how the HST compares against a Hohmann transfer. It then considers a launch from the Xichang Satellite Launch Centre in Sichuan province, China, which is China's main launch site for platforms bound for GEO, to investigate whether the HST can reduce the mass penalty associated with this high latitude launch site.

Transfer Specification	Property	
Launch Site	Guiana	Xichang
Launch Site Latitude, ΔI (°)	5.24	28.25
Initial Orbit GTO Perigee Radius, r_i (km)	6628	
Initial Orbit GTO Apogee Radius, r_t (km)	42,164	
Target Orbit Radius GEO, r_t (km)	42,164	
Mission Duration Limit, t_T (days)	90	
European Apogee Motor Specific Impulse, I_{spH} (s)	325	
T6 Thruster Specific Impulse, I_{spL} (s)	4500	
Gravitational Constant, μ (m^3/s^2)	3986004418×10^5	
Standard Gravitational Acceleration, g (m/s^2)	9.81	
Calculated Parameters		
Critical Specific Impulse Ratio, I_{sp}^{HHHE}	13.846	
R1	6.36	

Table 3 Launch site comparison using HST

Based on the data in Table 3, *R2* can be calculated for the Kourou launch site using Eq. (16) as 139.83, which is an intermediate orbit radius of approximately 22 GEO radii. From this, a range of wet masses can be derived depending on the propulsion capability on board such that the HST manoeuvre is equal to a 1-impulse at apogee high-thrust transfer, in terms of fuel mass fraction. The spacecraft is delivered to the target orbit within the ninety day timeframe as is shown in Figure 7.

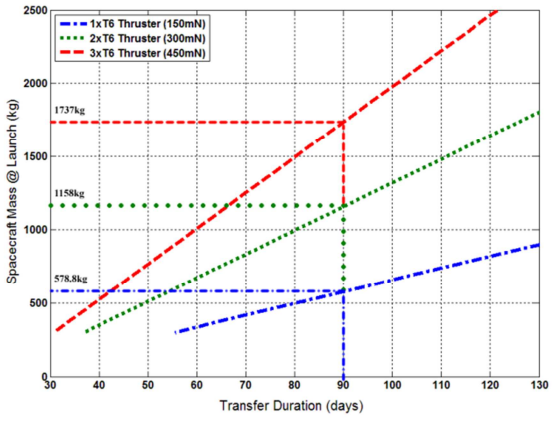

Figure 7 HST Wet Mass Capability from Korou Launch Site

If Xichang launch port is now considered with a wet mass of 578.8kg then, using the HST, it can be shown that the mass penalty associated with a high-latitude launch can effectively be eliminated.

[1] European Space Agency. *An Extended European Capability*. 2010; Available from: http://telecom.esa.int/telecom/www/object/index.cfm?fobjectid=1139

HST Breakdown	
Wet Mass, m_{wet} (kg)	578.8
Thrust, T (mN)	150
Mass after Phase 2, m_{02} (kg)	383.6
Dry Mass, m_{dry} (kg)	363.2
$R2$	139.83
Fuel Mass, m_{HSTF} (kg)	215.6

Table 4 Analysis breakdown of Spacecraft Launched from Kourou Launch Site

Considering Table 4, which details the breakdown of the HST transfer from the Kourou launch site, it can be seen that the fuel mass consumed is 215.6kg. Noting again that this is the same amount consumed as the high-thrust only transfer and considering Figure 8 which shows an analysis of a spacecraft with the same wet mass but launched from the Xichang site, it is shown that by using the HST with $R2$=147.4, which is an intermediate orbit of approximately 23 GEO radii, and a low-thrust system thrust of 154mN, the spacecraft can be delivered to GEO with the same dry mass as from the Kourou launch site in the 90 day timeframe. It should be noted that the thrust required is calculated using Eq. (28) which is a re-arranged version Eq. (27).

$$T = \frac{-m_{02}\left[gI_{spL}log\left(1-\frac{m_{HSTF}}{m_{wet}}\right)+\Delta V_{TIhigh}\frac{I_{spL}}{I_{spH}}\right]}{t_T-\frac{\pi}{\sqrt{\mu}}\sqrt{\left(\frac{rt(1+R2)}{2R1}\right)^3}} \qquad (28)$$

This translates as a mass saving of 37kg compared to the high-thrust only transfer from the Xichang launch site, as is shown in Figure 8. This means that users restricted to a high-latitude launch site can make a significant mass saving if launching to GEO orbit compared to the standard high-thrust transfer approach, or consider this mass saving as the creation of a 'virtual' launch site which mimics the advantages of a low latitude launch site at the expense of a slightly longer transfer.

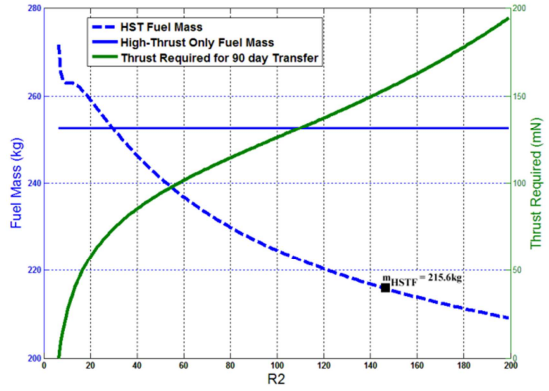

Figure 8 Analysis of a spacecraft with m_{wet} = 578.8kg from the Xichang Launch Site

Table 5 shows the analyses for the two other cases identified. It is shown that considering only the Xichang launch site, there is a significant mass saving available compared to the high-thrust only transfer. As before, the HST dry mass is equivalent to the high-thrust fuel mass required to achieve the target orbit from the Kourou launch site highlighting that by using the HST, there is no increase in fuel mass compared to the low-latitude launch site.

Spacecraft Mass, m_{wet} (kg)	**1158**	**1737**
High-thrust only Dry mass, m_{dry} (kg)	652.7	979.1
HST Dry mass, m_{dry} (kg) *(to equal that of the Kourou high-thrust dry mass)*	726.6	1089.9
Transfer time with specified thrust, t_T (days)	92.03 (300mN)	92.03 (450mN)
Low-Thrust System Thrust Required for ninety day Transfer, T (mN)	308.6	463.1
Mass Saving, (kg)	73.9	110.8

Table 5 Xichang Launch Site Analysis using HST

Numerical

Now considering the case study results using the numerical optimisation, which are compared to the analytical in Table 6, it can be seen that there are certain differences between the two methods. This is thought to be due to the analytical analysis assuming that no eccentricity control is required when in actual fact, as is shown by the numerical method in this section, some control is needed. Due to this the transfer time is approximately 120 days, 30 days more than calculated by the analytical. The fuel mass required is slightly more for all cases also, with the absolute error of the analytical compared to the numerical being approximately 4%. Although this error is significant, the mass saving, calculated by the numerical method is still substantial at roughly 5% of m_{wet} for all cases considered.

Spacecraft Mass, m_{wet} (kg)		**578.8**	**1158**	**1737**
HST Fuel mass, m_{HSTF} (kg)	Analytical	215.6	431.4	647.1
	Numerical	224.7	449.1	673.6
	Absolute Percentage Error (*w.r.t Numerical*) (%)	4	3.9	3.9
Transfer time with specified thrust, t_T (days)	Analytical	92.03 (150mN)	92.03 (300mN)	92.03 (450mN)
	Numerical	120.2 (150mN)	120.3 (300mN)	120.3 (450mN)
	Absolute Percentage Error (*w.r.t Numerical*) (%)	23.4	23.4	23.4
Mass Saving, (kg)	Analytical *(% of m_{wet})*	37 (6.4)	73.9 (6.4)	110.8 (6.4)
	Numerical *(% of m_{wet})*	27.9 (4.8)	56.2 (4.9)	84.3 (4.9)

Table 6 Numerical Results of Xichang Transfer

In order to understand the full transfer it is necessary to consider the trajectory profile. Figure 9 and 10 show the full HST transfer in 2D and 3D respectively. It should be noted that the high-thrust section has been added manually in both cases and only the low-thrust section has been numerically optimised. As discussed previously, the inclination change is performed by the HST's high-thrust section.

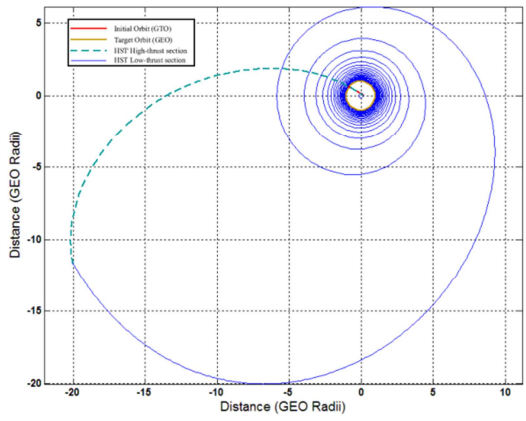

Figure 9 HST Trajectory Profile 2D

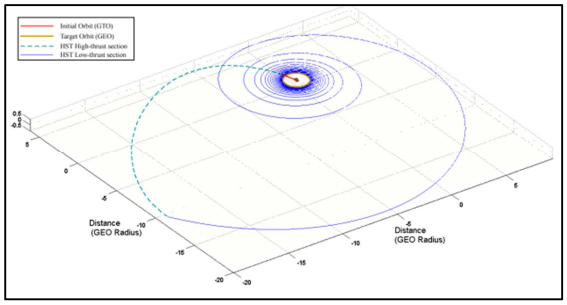

Figure 10 HST Trajectory Profile 3D

Figure 11 displays the HST low-thrust section spacecraft acceleration and highlights just how much eccentricity control is required. The profile begins on 19.85 days which is the end of the high-thrust section. It can be seen that in the first 40 days of the low-thrust section the transverse acceleration is continually dropping while the radial is increasing, this shows that there is substantial control of the eccentricity required at the beginning of this low-thrust phase. After this period, the majority of the acceleration is directed in the Transverse direction to lower the semi-major axis as expected. Figure 12 shows the history of the semi-major axis and eccentricity. It can be seen that the semi-major axis is constantly reducing as expected and the eccentricity history is in accordance with the Radial acceleration plot. This is due to a large eccentricity at the beginning and as such a large acceleration is required to overcome this.

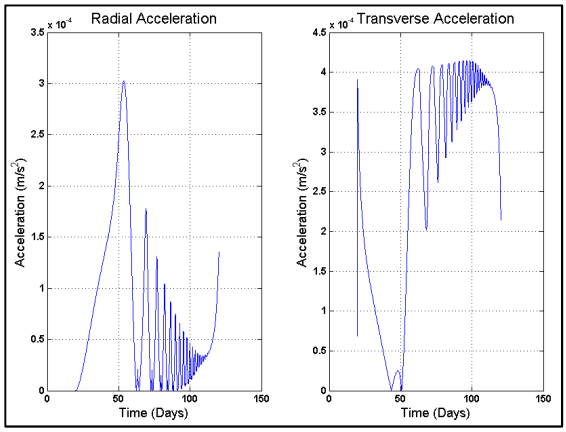

Figure 11 Low-Thrust Section Radial and Transverse Acceleration Profile History

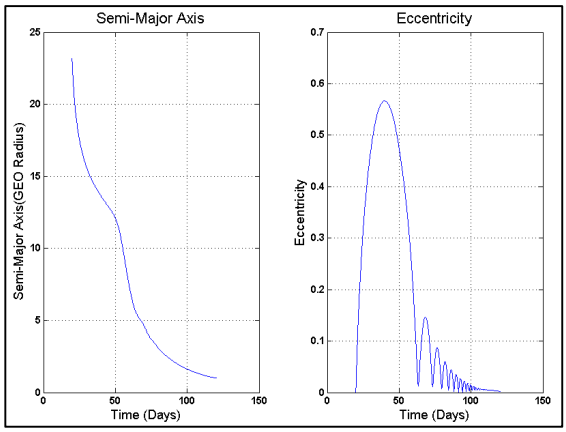

Figure 12 Semi-Major Axis and Eccentricity Low-Thrust Section Profile History

X.CONCLUSION

The previously defined Hohmann spiral transfer has been extended from a co-planar analysis to incorporate a plane change. A numerical analysis validated the analytical approach for a low *R2* value, however a case study considering a GTO-GEO transfer has shown that with certain spacecraft configurations there can be a significant difference between the analytical and numerical studies due to some eccentricity control being required to prevent the spacecraft entering a rectilinear orbit. Therefore, although the analytical approach gives a good indication of the HST characteristics, the numerical approach should be used to give an accurate representation of the transfer. It was found that with a large inclination change the HST's efficiency is greatly improved and can outperform the compared transfer at relatively low R2. By considering a transfer from a launch site latitude of ≈28° (China) to GEO, a mass saving of 5% of m_{wet} can be achieved within a transfer time of ≈ 120 days, compared to the high-thrust only transfer. This 5% saving means the fuel mass required is equivalent to a spacecraft with the same parameters launched from a latitude of ≈6° to GEO (Kourou), suggesting the HST can be used to mimic low-latitude launch sites and eliminate the mass penalty associated with high-latitude launch sites at the expense of a longer transfer duration.

XI.REFERENCES

[1] S. Owens and M. Macdonald, "An Analogy to Bi-Elliptic Transfers Incorporating High and Low-Thrust," *Journal of Guidance, Control, and Dynamics (In Press)*, 2012.

[2] D. Y. Oh, T. Randolph, and S. Kimbrell, "End to End Optimization of Chemical-Electric Orbit Raising Missions," *Journal of Spacecraft and Rockets*, vol. 41, no. 5, pp. 831–839, 2004.

[3] D. Y. Oh and G. Santiago, "Analytic Optimization of Mixed Chemical-Electric Orbit Raising Missions," *27th International Electric Propulsion Conference, IEPC Paper 01-173*. Pasadena, California, USA, 2001.

[4] D. Y. Oh and S. Kimbrell, "End to End Optimization of Three Dimensional Chemical-Electric Orbit Raising Missions," *28th International Electric Propulsion Conference, IEPC-03-036*. Toulouse, France, 2003.

[5] R. S. Gershman C, "Propulsion Trades for Space Science Missions," *Third IAA Conference on Low-Cost Planetary Mission*. Pasadena, CA, 1998.

[6] J. E. Y. and R. G. Choueiri, "Electric Propulsion," *Encycolpedia of Physical Science and Technology*, vol. 5. Academic Press, pp. 125–141, 2002.

[7] M. G. Lyszyk P, "Electric Propulsion System on @BUS Platform," *4th int. Spacecraft Propulsion Conference*. Cgliari, Sardinia, Italy, 2004.

[8] D. A. Vallado, *Fundamentals of Astrodynamics and Applications*, 3rd ed. Microcosm Press and Springer, 2007, pp. 353–354.

[9] D. A. Vallado, *Fundamentals of Astrodynamics and Applications*, 3rd ed. Microcosm Press and Springer, 2007, p. 354.

[10] M. J. Sidi, *Spacecraft dynamics and control: a practical engineering approach*, Cambridge . Cambridge University Press, 1997, pp. 73–76.

[11] S. Loney, *Plane Trigonometry*. Cambridge: University Press, 1893, pp. 173–183.

[12] M. J. H. Walker Ireland, B and owens, J, "A Set of Modified Equinoctial Orbit Elements," in *Celestial Mechanics 36*, D. Reidel Publishing Company, 1985, pp. 409–419.

[13] M. Macdonald, "Analytical Methodologies for Solar Sail Trajectory Design," University of Glasgow, Glasgow, 2005.

[14] C. Kluever, "Simple guidance scheme for low-thrust orbit transfers," *Journal of Guidance Control and Dynamics*, vol. 21, no. 6, pp. 19–21, 1998.

[15] J. Schoenmakers, J. Pulido, and R. Jehn, "ESOC report S1-ESC-RP-5001."

[16] J. Nocedal and S. J. Wright, *Numerical Optimization*. Springer, 2003, pp. 77–94.